A Positron Camera Using Position-Sensitive Detectors: PENN-PET

Gerd Muehllehner and Joel S. Karp

Department of Radiology, Hospital of the University of Pennsylvania, Philadelphia, Pennsylvania

A single-slice positron camera has been developed with good spatial resolution and high count rate capability. The camera uses a hexagonal arrangement of six position-sensitive NaI(Tl) detectors. The count rate capability of NaI(Tl) was extended to 800k cps through the use of pulse shortening. In order to keep the detectors stationary, an iterative reconstruction algorithm was modified which ignores the missing data in the gaps between the six detectors and gives artifact-free images. The spatial resolution, as determined from the image of point sources in air, is 6.5 mm full width at half maximum. We have also imaged a brain phantom and dog hearts.

J Nucl Med 27:90–98, 1986

Compared with other medical imaging techniques such as x-ray computed tomography and magnetic resonance imaging, nuclear medicine has continued to suffer from inferior image quality, which has largely been the result of limitations imposed by mechanical collimation necessary to form an image with single-photon emitters. This basic limitation can be overcome to a large degree by using positron-emitting radiotracers and detecting the two gamma-rays which are emitted following annihilation of the positron.

Positron imaging instruments have been under development for many years (*1–3*). However, in the last few years the imaging characteristics have improved dramatically to the point where present state-of-the-art whole-body systems have spatial resolution of 8 mm full width at half maximum (FWHM) or better, image several contiguous transverse slices simultaneously and have sufficient sensitivity to result in high quality images in a reasonable imaging time (*4–6*). This performance has only been achieved through increased complexity to the point where some systems now have more than 500 individual scintillation detectors and photomultipliers (*5*).

In order to avoid the complexity and therefore the high cost of positron cameras, we have investigated the use of position-sensitive detectors for positron imaging. Various problems, some specific to this design, have been investigated with a single-slice system which is now completed and which will be described in detail below. Extension of the approach to a multislice system is currently under investigation.

Received Apr. 10, 1985; revision accepted Sept. 18, 1985.

For reprints contact: Gerd Muehllehner, PhD, Dept. of Radiology, Hospital of the University of Pennsylvania, Philadelphia, PA 19104.

SYSTEM DESCRIPTION

The PENN-PET positron camera uses a hexagonal arrangement of six position-sensitive detectors (Fig. 1). Each detector incorporates a scintillation crystal of NaI(Tl) which is 500 mm long, 50 mm wide, and 25 mm thick. The crystal is coupled to ten photomultipliers of 50 mm diameter which are connected to a resistive divider network to provide a position-dependent signal. Each detector is in coincidence with three opposing detectors to permit the recording of coincident gamma-rays from any location in the patient aperture which is 50 cm in diameter. The detectors are shielded to image a single slice with a maximum width of 26 mm (i.e., FWHM = 13 mm).

Detectors

Continuous detectors have two principal advantages in positron systems.

1. They provide continuous sampling, thereby eliminating the need for moving the detectors.

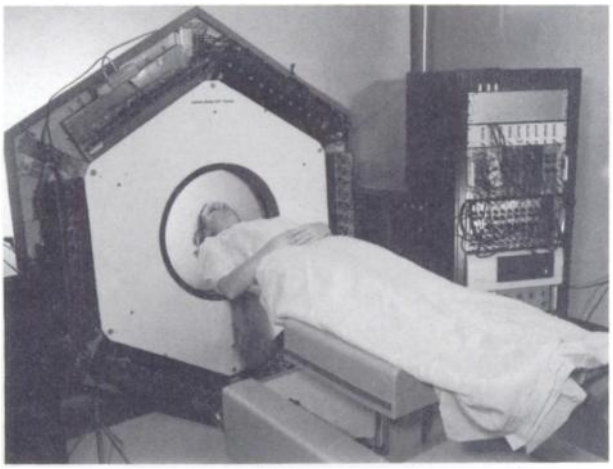

FIGURE 1
Photograph of positron camera

2. They minimize loss of sensitivity which occurs at the edge of detectors and which therefore increases as discrete detectors are made smaller to improve spatial resolution (*7*).

Practically all positron imaging systems incorporate some kind of motion in order to achieve sufficient linear and angular sampling. Considerable ingenuity has been displayed to arrive at simple mechanical movements such as "wobbling" (*8,9*), continuous rotation (*10*), dichotomic (*11*), "clam-shell" (*12*), and translate and rotate (*13*) motion. If a small source is moved transversely to the line between a stationary detector pair, the recorded position will not change, but the intensity will change depending on the exact location. This sampling problem was encountered in the Donner ring (*12*), and it was shown that sharp edges of objects are distorted even if 280 detectors are used in a ring. The problem can be reduced by either using one of the above-mentioned motions or decreasing the size of the detectors still further (*5*). However, no matter how many detectors are used, if discrete detectors are held stationary, the system is undersampled relative to the size of the detectors used even if adjacent angular projections are summed (*14*). A continuous detector avoids this problem since the digitization resolution can easily be made a small fraction of the spatial resolution. Even if the source is a small fraction of the spatial resolution, the recorded intensity is not a function of position, and a small lateral shift of the source can easily be detected.

High spatial resolution with a continuous detector can be obtained with relatively few photomultipliers through interpolation of signals from individual tubes as has been first demonstrated by Anger (*15*) for scintillation imaging and which is also widely used in other position-sensitive detectors such as proportional counters (*16*). In our approach we sum all photomultiplier tube signals with equal weight to obtain a signal which is proportional to the total energy deposited in the crystal and also sum all signals with different weights to obtain a signal which is proportional to the position at which the scintillation occurred. This summing method effectively finds the centroid of the light emitted in the scintillation crystal. The accuracy of position determination using this method is a small fraction of the diameter of the photomultiplier. A different method to determine the centroid which uses many small BGO crystals and requires more complex electronic circuitry has been developed by Brownell et al. (*17*).

The detectors used in our positron camera consist of bars of NaI(Tl) 500 mm long, 50 mm wide, and 25 mm thick, each coupled to ten 50-mm diameter phototubes through a 12.5 mm thick piece of pyrex. The ends of the crystal are beveled at 30° to permit close packing of six detectors in a hexagonal ring. For each gamma-ray interaction, the emission of scintillation light results in a distribution of light at the plane of the photocathodes which is peaked near the point of incidence. The position X along the long axis of the crystal is determined from the centroid of the light distribution; $X = \Sigma x(i)E(i)/\Sigma E(i)$ where i is the phototube number, x(i) is the position of the center of the phototube, and E(i) is the phototube signal.

The accuracy with which the position is calculated determines the spatial resolution ΔX. The resolution is inherently limited by the localization of energy deposition which spreads by Compton scattering. The amount of scattering in the crystal depends on the gamma-ray energy, the crystal stopping power, and its thickness. The resolution is affected, to a greater degree, by the statistical fluctuations of the phototube signals, which depend upon the light output of the crystal and the conversion efficiency of the photocathodes. Sodium iodide was chosen for its very high light output to minimize statistical fluctuations and for its high stopping power to minimize Compton scattering. A high stopping power, and therefore high efficiency is essential in a crystal designed for use in a positron tomograph. Other scintillators with even higher stopping power (e.g., CsF, BaF_2, BGO) have very low light output compared to NaI(Tl). BGO has the highest light output of those mentioned, which is less than one-sixth that of NaI(Tl). In a continuous position-sensitive detector such as ours, a high spatial resolution could not be achieved with such a low light output. Since NaI(Tl) has a long decay time (0.24 μsec), however, delay line pulse shortening is employed when high count rates are encountered, as will be described in the next section. This results in a degradation in spatial resolution since only one-third of the light emitted in NaI(Tl) is integrated. Even with pulse shortening, however, the effective light output of NaI(Tl) is considerably higher than that of other scintillators.

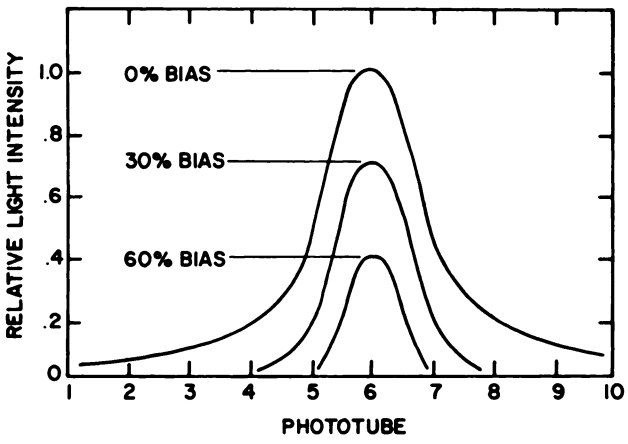

FIGURE 2
After-bias light distribution as function of percent bias with collimated source of gamma-rays incident over phototube 6

Because of the statistical fluctuations of the phototube signals, the width of the light distribution also affects the resolution. While the light which is received by phototubes far from the point of scintillation contains little position information, the statistical uncertainty of these phototube signals seriously degrades the spatial resolution. One method of sharpening the light distribution in order to improve the resolution is through the use of nonlinear preamplifiers. A bias circuit is used to subtract from the signal a constant voltage bias (*18*) which constitutes an increasing fraction of the phototube signal as the distance from the interaction site increases. This has the effect of minimizing the contribution of low-level signals. Figure 2 shows this effect as a function of percent bias, which is defined as the percentage of the signal which is subtracted from a phototube when an event occurs directly over its center. Here, a collimated source of gamma rays is incident directly over the center of phototube 6. The curve labeled 0% is the before-bias light distribution. With a bias of 30% the tails of the light distribution are reduced to the extent that the position is determined mainly by three phototubes. This bias is found to be optimal in terms of spatial resolution. As the bias increases beyond 30%, fewer phototubes contribute to the position signal and the resolution worsens.

The bias circuit also affects the spatial linearity. Even without bias, the measured position is only approximately a linear function of the source position. As the percent bias increases, the measured position becomes increasingly insensitive to the source position near the center of each phototube. Although moderate nonlinearities, such as those at 30%, can be corrected for with software (*19*), severe distortions, such as those at 60%, cannot.

This detector configuration was studied both experimentally and by simulating a variety of detector configurations which is described in more detail elsewhere (*20*).

Three representative position spectra both with and without pulse shortening are shown in Fig. 3A, taken at positions 12.5 mm apart. The average resolution, $\overline{\Delta X}$, is calculated from measurements every 6.3 mm between phototubes 5 and 6. The resolution of each peak is calibrated using the peak positions of the two adjacent measurements. The resolution (FWHM) is 6.2 mm

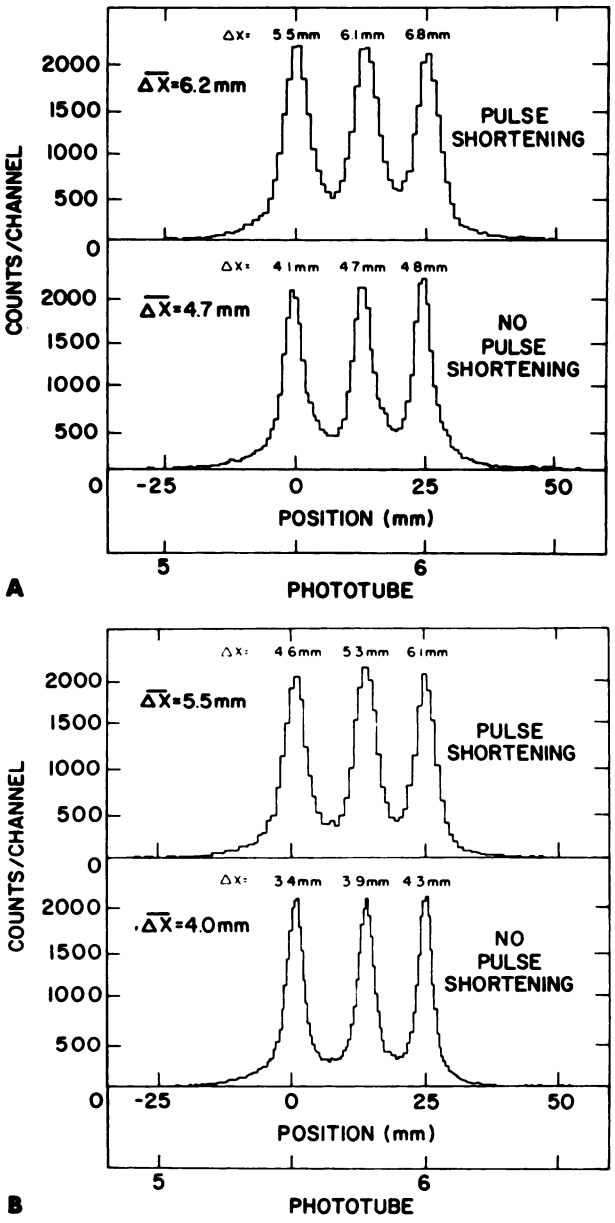

FIGURE 3
A: Position spectra taken with diffuse scintillation crystal, with and without pulse shortening. Gamma-rays are incident on crystal at positions X_0 = 0, 12.5 and 25 mm. B: Position spectra taken with grooved crystal, with and without pulse shortening. Gamma-rays are incident on crystal at X_0 = 0, 12.5 and 25 mm

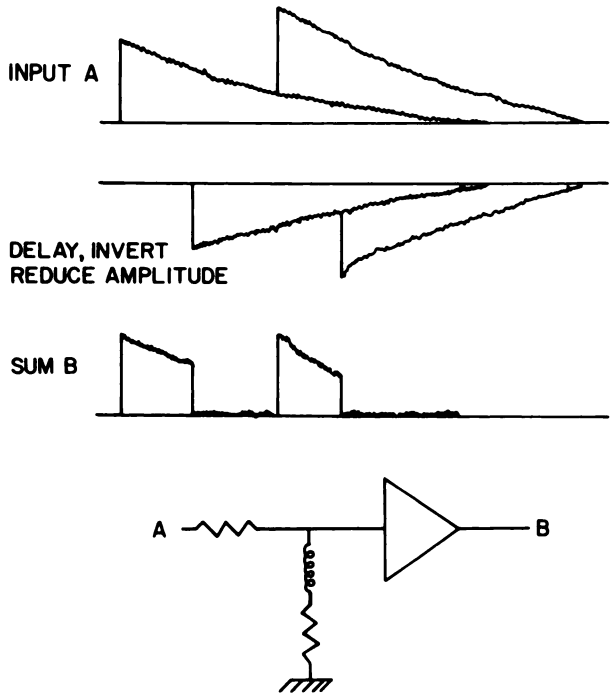

FIGURE 4
Light intensity emitted from NaI(Tl) decays exponentially and may overlap if scintillations occur within short time interval (top). Pulse shortening can subtract much of exponential tail and thus avoid pulse pile-up (middle). Relatively simple circuit consisting of delay line and two resistors at input to preamplifier is used to shorten pulses (bottom)

with pulse shortening and 4.7 mm without, at a bias of 30%. The uncertainty of these values is ±0.2 mm.

The spatial resolution is taken as the FWHM of the curve, although the position spectra have somewhat wider tails than Gaussian curves. In addition to the effect of Compton scattering in the crystal, gamma-rays scattering from the collimator or passing through the lead slit contribute to these tails.

A technique which affects the resolution is to vary the shape of the light distribution itself. Although the bias threshold can effectively narrow the light distribution, an intrinsically narrow light distribution results in better statistics for the phototubes near X_0. The width of the distribution is most sensitive to reflections from the front surface of the crystal (opposite the phototubes).

In an effort to prevent broadening of the light distribution without losing the light emitted towards the front face of the crystal, we investigated modifying the surface by cutting 2-mm-deep grooves perpendicular to the long dimension of the crystal. This has the effect of redirecting the light back towards its origin, resulting in a narrow light distribution. The position spectra measured with the grooved crystal are displayed in Fig. 3B. Here the values $\overline{\Delta X}$ improve to 5.5 and 4.0 mm with and without pulse shortening, respectively. Monte Carlo simulations have enabled us to vary detector parameters to predict their effect on spatial resolution and to study the physics limiting the resolution. While we have made significant improvements since this investigation began, we believe that the spatial resolution of this detector can be improved still further, perhaps with better electronics.

Count Rate Capability

Since all counts from a bar detector are processed sequentially through a single chain of electronics, it is necessary to process large count rates. It has previously been estimated (*21*) that up to 700,000 cps will have to be processed from each detector with counting losses below 20%. After a gamma-ray interacts in NaI(Tl), the resulting light is emitted with a decay time of 240 nsec and requires 1,000 nsec for 98% light collection. Without special pulse handling techniques, this slow decay will result in pulse pileup at high data rates and seriously limit the count rate capability achievable with NaI(Tl). Higher count rates can be achieved with other scintillators such as CsF or BaF_2; however, the low light output makes it difficult to obtain accurate position determination in a continuous detector. A number of methods have been described to significantly increase the count rate capability of NaI(Tl) detectors at some loss of energy and position resolution (*21–24*). We have elected to use pulse shortening to subtract the exponential tail of the pulse (Fig. 4) and a constant integration time of 120 nsec. Pulse shortening uses less light output resulting in greater statistical uncertainty and worse positional resolution. Tanaka et al. (*23*) have described a variable integration time technique after pulse shortening which would avoid much of the spatial resolution loss encountered with a fixed integration time. Implementing a variable integration time with sufficient accuracy is not an easy task but represents a desirable improvement over the method we have currently implemented.

Table 1 shows the fraction of light collected as a function of integration time. With an integration time of 120 nsec, more than one-third of the total light emitted is collected and integrated. Using passive pulse shaping, the total deadtime can be kept to ~250 nsec. Coincidence timing is derived from the unintegrated

TABLE 1

Integration time (nsec)	Fraction of light emitted
50	19%
100	34
240	63
400	81
1,000	98

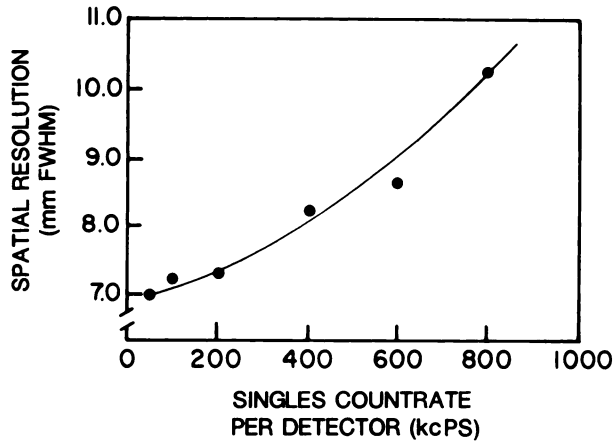

FIGURE 5
Loss of spatial resolution as function of measured singles rate on detector before subtraction of randoms

charge pulse, and the integrated pulse is peak sampled. At an input rate of 700,000 cps, less than 20% of all pulses occur within a time interval of 250 nsec (*25*). It is unlikely that we will encounter a clinical situation where the singles rate will exceed 700,000 cps per detector. The loss of spatial resolution measured with a line source placed midway between two bar detectors is shown in Fig. 5 as a function of the measured singles rate. As the input rate increases, the spatial resolution degrades due to a number of different factors. While pulse shortening returns the electronic signal to an average value of zero, the statistical fluctuations in the pulse being shortened causes the baseline to be noisy. Scintillations occurring within 1,000 nsec of another scintillation in the same crystal therefore suffer some loss of spatial resolution. Random coincidence counts add a background which increases at elevated count rates and which appears as a broadening of the FWHM since randoms have not been subtracted to obtain the values shown in Fig. 5.

IMAGE RECONSTRUCTION

The position of a scintillation event along a detector is recorded as an 8-bit binary number at the output of analog-to-digital converters. Therefore, each detector can be thought of as being divided into 256 equal elements or intervals. Each detector is in coincidence with three detectors on the opposite side, thus nine coincident detector pairs are possible between all six detectors. For each coincident event detected, the position coordinates of the respective detectors are digitized, and the event is recorded by incrementing a memory location in a two-dimensional (256 × 256) matrix by one count. Since each coincident detector pair has a 256 × 256 matrix associated with it, a total of more than 500 Kbytes of random access memory are required to store the incoming information in this unprocessed form.

To reconstruct transverse section images, spatial distortions in the detectors must be compensated for, the data matrices must be compressed to make them more manageable, and a reconstruction algorithm must be used which compensates for the missing data caused by the physical gaps between the scintillation detectors.

Distortion Removal and Data Reorganization

Spatial distortions are systematic errors in the positioning of scintillation events. Each event results in a distribution of light at the plane of the photocathodes. The centroid of this distribution, as measured by the phototubes, is used to define the position of the event. The measured position, however, is only approximately a linear function of the true position because the light distribution is sampled only every 50 mm and also because of nonlinear effects near the edges of the crystal. In addition, the differential and integral nonlinearities of the analog-to-digital converters contribute to the spatial distortions.

Since there is a one-to-one correspondence between the measured and true positions, the spatial distortions can be measured and compensated for (*19*). This correction is achieved in practice by collimating a line source placed at the center of the patient aperture and using a lead ring which has 90 equidistant slits. This type of collimator allows narrow beams of gamma rays to strike the detectors at known positions. Since the actual positions of the coincident gamma-rays on the detector surface are known, the distortion factors can be computed by taking the difference between the measured and the actual positions. We obtain 360 factors (one distortion factor per degree) by rotating the lead ring four times in one-degree increments. This allows us to calculate the distortion factors at 8-mm intervals along the detector. The complete distortion lookup table is formed by linearly interpolating values between the measured points, since the distortions change smoothly and linearly over short distances.

Figure 6 shows data from a number of point sources which have been rebinned into polar coordinates both without (Figs. 6A and 6B) and with (Figs. 6C and 6D) distortion removal. A convenient way of reorganizing the data is a coordinate transformation to polar coordinates with the center of the patient port as its origin. This simple coordinate transformation reduces the memory requirements significantly and organizes the data into a form which is convenient for reconstruction algorithms. Ideally, any point source describes a sinusoidal curve; the deviations from this shape are clearly visible if no distortion removal is employed. Figures 6A and 6C show the reconstructed images using the data sets corresponding to Figs. 6B and 6D, respectively. The reconstructions were obtained with an iterative

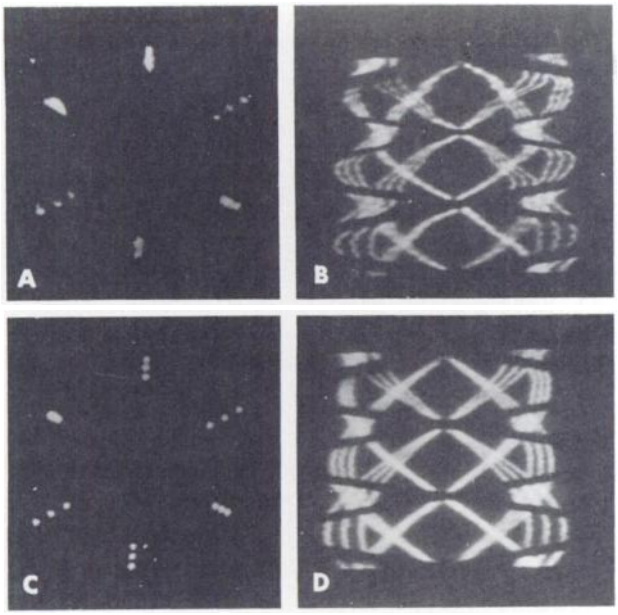

FIGURE 6
Reconstructed images of several point sources without distortion removal (A) and with distortion removal (C) together with the corresponding projection data (B and D, respectively). Separation of point sources is 10 mm (12 o'clock), 20 mm (2 o'clock), 8 mm (4 o'clock), 12 mm (6 o'clock), 20 mm (8 o'clock) and 6 mm (10 o'clock)

algorithm which will be described in the next section. As can be seen, accurate distortion removal is essential to obtaining high resolution, artifact-free images.

When imaging extended objects, it is necessary to compensate for any nonuniformity in the data. This is caused by the nonuniformity of response along the detectors as well as the nonuniformity due to the truncation errors and mapping during the rebinning process. Data taken with a rotating line source are used to calculate uniform projection data which then allows us to normalize the data of interest.

Distortion removal and rebinning can be performed by an on-line processor in real time, and such a processor has recently been designed and built for our system (*26*). On-line rebinning reduces the memory requirements sufficiently to permit multiframe data acquisition for gated cardiac imaging.

Reconstruction Algorithm

Since the ring of six detectors is totally stationary, it is necessary to compensate for the data which are missing due to the gaps between the detectors. The physical space between the scintillation crystals has been minimized as much as possible; however, the last 10 mm at either end of the crystal have large spatial distortions and are not useful for gamma-ray localization. Including the actual separation between the detectors, the gap in the data corresponds to a 6° angular range. The total data loss for all six gaps is therefore 10% of the total angular range and results in a 20% reduction in coincidence detection efficiency. The effect of the gaps can be seen in the projection data of Fig. 6 as diagonal bars of missing data.

Iterative algorithms reconstruct an image which is consistent with a particular data set without requiring a complete data set. A number of investigators have studied the effect of incomplete data on image quality using a variety of algorithms (*27–29*). Almost any iterative algorithm can be easily modified to exclude elements in the projection data which correspond to the gaps between detectors.

The results presented here were obtained with a modified version of the maximum likelihood (ML) algorithm (*30,31*), but other algorithms have been evaluated (*32*) using the same data. The ML algorithm is a multiplicative algorithm which updates the estimated image once per iteration. It converges more slowly than others (*32*) but is not as susceptible to inconsistencies in the data arising from statistical noise (*31*). More complete discussion of this algorithm and its application to our positron camera, are published elsewhere (*30, 31,33, 34*).

The ability of the ML algorithm to reconstruct artifact-free images using incomplete data was studied using both simulated and real data. Projection data were calculated for a Derenzo phantom with a simulated spatial resolution of both 7 mm FWHM and 4 mm FWHM. Figure 7 shows reconstructed images using the ML algorithm on simulated projection data without

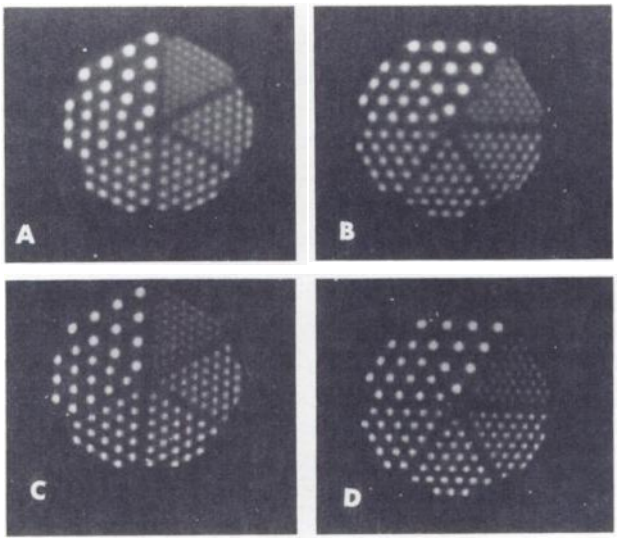

FIGURE 7
Reconstruction of simulated data with 7-mm system resolution (A and B) and 4-mm system resolution (C and D). Images on left (A and C) are reconstructed from complete data set, images on right (B and D) have six data gaps corresponding to 6° angular range each

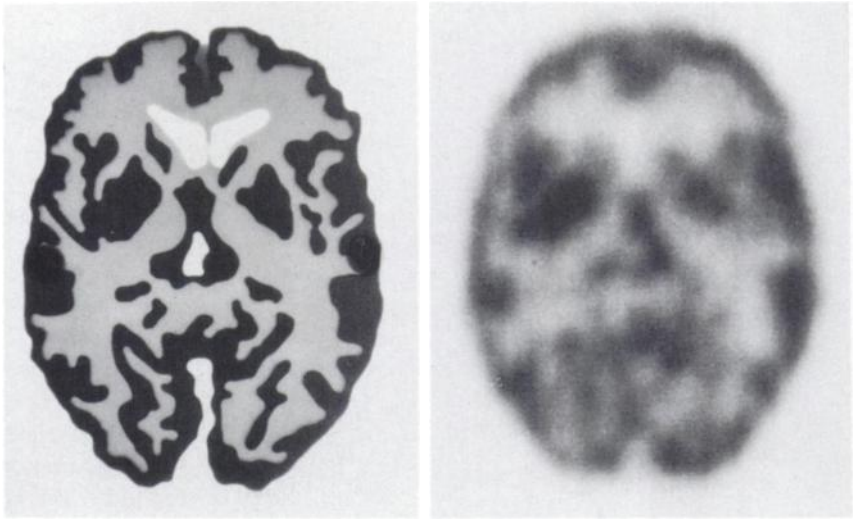

FIGURE 8
Photograph of "Hoffman" brain phantom (left) and image of phantom after it was filled with 300 μCi ^{18}F and imaged for 20 min

statistical noise added both with and without gaps in the data. In the particular orientation shown in these images, the gaps do not produce noticeable artifacts. However, if the phantom is rotated 30° with respect to the gaps, then critical, high-frequency components of projection data are eliminated, and some artifacts are noticeable. This is due to the highly symmetrical structure of this particular phantom and is not likely to cause a problem in more realistic objects.

SYSTEM PERFORMANCE

The image of point sources in air (Fig. 6) gives a good indication of the system performance under ideal conditions. The sources separated by 8 mm are clearly resolved; the measured resolution from profiles through these sources is 6.5 mm FWHM. This performance was achieved with each of the system's six detectors having an intrinsic resolution of 6.0 mm rather than the best measured value of 4.0 mm, as mentioned earlier. This is true as well for the images discussed below. In positron tomographs consisting of a circular array of individual detectors the spatial resolution is best at the center and degrades towards the perimeter of the field-of-view, particularly in the radial direction, due to the uncertainty of the depth of interaction in the scintillator. In our positron emission tomographic (PET) camera there is some loss of spatial resolution due to the uncertainty of the depth of interaction throughout the field-of-view, but the resolution does not vary appreciably as a function of the distance from the center. Quoting a system resolution for emission computed tomographic (ECT) systems is not as simple as for planar imaging devices. If a filtered back projection reconstruction algorithm is used, then the system resolution is a function of the filter; if an iterative reconstruction algorithm such as the ML algorithm is used, then the reconstructed resolution is dependent upon the object distribution and the number of iterations. Even though the results shown in Fig. 6 and Fig. 8 were both obtained with 16 iterations, the image resolution is not the same. At the present time, it is not clear how to assign a numerical value to the image resolution when a complex object such as shown in Fig. 8 is imaged.

The sensitivity of the system was measured with a cylinder of activity 20 cm in diam centered in the field-of-view and was found to be 7,000 cps/μCi/cc after subtraction of random coincidences. An energy discriminator excludes events which are not photopeak events. This sensitivity is lower than other whole-body positron cameras using either thicker scintillators or materials with a higher stopping power such as BGO. Increasing the thickness of the scintillator leads to a poorer spatial resolution (*20*). Since poorer spatial resolution would necessitate the accumulation of more counts for equal image quality (*35*), no overall benefit can be obtained by increasing the thickness of the scintillator unless some method can be found to avoid the accompanying loss of resolution. Note, however, that the sensitivity is approximately ten times higher than can be achieved with single photon ECT systems.

Figure 8 shows a photograph of the "Hoffman" phantom (*36*) and an image of the phantom. The Hoffman phantom is a realistic representation of the activity distribution in the brain after administration of fluorine-18 fluorodeoxyglucose ([^{18}F]FDG) with a ratio of "gray matter" to "white matter" of 4:1. The phantom was filled with <0.3 mCi of ^{18}F which corresponds to the level of activity found in human subjects after administration of 8 mCi of FDG. The image acquisition time was 22 min and 4.8 million counts were collected. At the low data rates typical of equilibrium imaging, the random coincidence events are less than 1% of the true coincidence events.

To test the performance of the system at high count rates, we injected 30 mCi of rubidium-82 (^{82}Rb) into

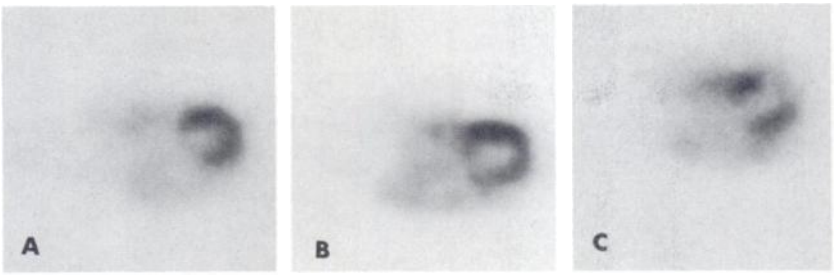

FIGURE 9
Myocardial images of three dogs after infusion of 30 mCi of ^{82}Rb. Singles rate was ~180k cps at start of imaging. A and B show normal myocardial uptake; C shows infarct due to ligation of left anterior descending coronary artery. Anterior is to right

dogs and started imaging the heart 60 sec after end of infusion to allow for blood clearance and continued until the ^{82}Rb had essentially decayed. Since ^{82}Rb has a half-life of only 75 sec, the countrates vary over a wide range during data collection. At the beginning of imaging the singles rates per detector were 180,000 cps, the total coincidences were 16,000 cps and for the coincidence resolving time of 16 nsec the calculated randoms fraction (randoms/true coincidences) was 24% (excluding random coincidences projecting outside the patient port). During data acquisition, the random fraction decreased rapidly so that the average random rate was significantly lower. Figure 9 shows myocardial images of three dogs. Two dogs (Figs. 9A and 9B) were imaged without intervention; the third (Fig. 9C) had the left anterior descending coronary artery ligated to create a myocardial infarct. Uptake in normal myocardial tissue is clearly delineated; the relatively pronounced lung uptake could be reduced by starting imaging at a later time but only at a loss of counts in the myocardium. One of the advantages of ECT is the fact that the lung activity does not interfere with visualization of the myocardium.

DISCUSSION AND SUMMARY

A single-slice positron camera has been developed with good spatial resolution, high sensitivity and count rate capability adequate for even demanding equilibrium studies. In developing it, two major problems had to be solved: the count rate capability achievable with NaI(Tl) had to be extended significantly and a reconstruction algorithm had to be developed which is insensitive to the missing data resulting from the gaps between the detectors. The former problem was solved through the use of pulse shortening which permits imaging at singles count rates up to 800k cps. To solve the problem of the missing data, we could have chosen to rotate the detectors during data acquisition; in order to preserve the simplicity of the system and keep the detectors stationary, we instead modified an iterative algorithm which ignores the missing data and gives artifact-free images with most objects imaged to date. In addition, we spent considerable time optimizing the performance of the bar detector used in the camera. If we modified the system's detectors with the improvements which led to an intrinsic detector resolution of 4 mm, we would expect the overall system resolution to be 5 mm or better.

To extend the concepts to a multislice system, two solutions come to mind: either identical single-slice rings can be stacked or, instead of a one-dimensional bar detector, a rectangular, two-dimensional area detector can be designed. In either case shielding can be used to reduce the scattered radiation to an acceptable level. We are currently exploring the latter possibility since it has the advantage that equal resolution can be achieved in all three directions with spatial sampling which is finer than the resolution.

In the approach described here, some performance has been sacrificed, particularly in sensitivity, in order to maintain simplicity of design. The overall goal has been to design a system which is potentially useful and affordable for clinical nuclear medicine. Clearly, PET scanners can have better spatial resolution and higher sensitivity than single photon ECT devices as has been shown above. Before a positron camera can become a useful clinical tool, appropriate radiopharmaceuticals must become available. So far, many positron-emitting radiopharmaceuticals have been developed at research centers with medical cyclotrons which use oxygen-15, nitrogen-13 or carbon-11. These are unlikely to find widespread clinical use due to their short half-life (20 min or less) and the high cost of cyclotrons. Longer-lived or generator-produced positron radiopharmaceuticals have received less attention due to the lack of appropriate instrumentation to image them. The strontium-82/rubidium-82 generator is a notable exception, however; its commercial implementation is actively being pursued at present. It is hoped that the development of clinically affordable instruments as the one described here will stimulate the development of other appropriate positron radiopharmaceuticals.

ACKNOWLEDGMENTS

This work is supported by the Department of Energy under contract DE-AC02-80EV10402. Drs. James Colsher, Robert M. Lewitt and Albert Guvenis have provided significant assistance which we gratefully acknowledge.

REFERENCES

1. Anger HO, Davis DH: Gamma-ray detection efficiency and image resolution in sodium iodide. *Rev Sci Instrum* 35:693-697, 1964
2. Brownell GL, Sweet WH: Localization of brain tumors with positron emitters. *Nucleonics* 11:40-45, 1953
3. Rankowitz S, Robertson JS, Higinbotham WA, et al: Positron scanner for locating brain tumors. *IRE Int Convent Rec* 9:49-56, 1962
4. Ter-Pogossian MM, Ficke DC, Yamamoto M, et al: Super PETT-I: A positron emission tomograph utilizing photon time-of-flight information. *IEEE Trans* MI-1:179-192, 1982
5. Hoffman EJ, Ricci AR, van der Stee LM, et al: ECAT-III-Basic design considerations. *IEEE Trans* NS-30:729-733, 1983
6. Takami K, Ueda K, Okajima K et al: Performance study of whole body, multislice positron computed tomograph—Positologica-II. *IEEE Trans* NS-30:734-738, 1983
7. Derenzo SE, Budinger TF, Huesman RH: Detectors for high resolution dynamic positron emission tomography. In *The Metabolism of the Human Brain Studied with Positron Emission Tomography*, Greitz T, et al, eds. New York, Raven Press, 1985, p 21
8. Bohm C, Eriksson L, Bergstrom M, et al: A computer assisted ring detector positron camera system for reconstruction tomography of the brain. *IEEE* NS-25:624-637, 1978
9. Ter-Pogossian MM, Mullani NA, Hood JT, et al: Design considerations for a positron emission transverse tomography (PETT V) for imaging of the brain. *J Comput Assist Tomogr* 2:539-544, 1978
10. Nohara N, Tanaka E, Tomitani T, et al: Positologica: A positron ECT device with a continuously rotating detector ring. *IEEE* NS-27:1128-1136, 1980
11. Cho ZH, Hong KS, Ra JB, et al: A new sampling scheme for the ring positron camera: Dichotomic ring sampling. *IEEE* NS-28:94-98, 1981
12. Derenzo SE, Budinger TF, Huesman RH, et al: Imaging properties of a positron tomograph with 280 BGO crystals. *IEEE* NS-28:81-89, 1981
13. Hoffman EJ, Phelps ME, Mullani NA, et al: Design and performance characteristics of a whole-body positron transaxial tomograph. *J Nucl Med* 17:493-502, 1976
14. Huesman RH, Cahoon JL: Data acquisition, reconstruction and display for the Donner 280-crystal positron tomograph. *IEEE* NS-27:474-478, 1980
15. Anger HO: Scintillation camera. *Rev Sci Instrum* 29:27-33, 1958
16. Borkowski CJ, Kopp MK: Design and properties of position-sensitive proportional counters using resistance-capacitance position encoding. *Rev Sci Instrum* 46:951-962, 1975.
17. Brownell GL, Burnham CA, Chesler DA, et al: PCR-I-High resolution positron tomograph using analog coding. *IEEE Trans* MI-3:10-16, 1984
18. Kulberg GH, van Dijk N, Muehllehner G: Improved resolution of the Anger scintillation camera through the use of threshold preamplifiers. *J Nucl Med* 13:169-171, 1972
19. Muehllehner G, Colsher JG, Stoub EW: Correction for field nonuniformity in scintillation cameras through removal of spatial distortion. *J Nucl Med* 21:771-776, 1980
20. Karp JS, Muehllehner G: Performance of a position-sensitive scintillation detector. *Phys Med Biol* 30:643-655, 1985
21. Muehllehner G, Colsher JG: Use of position sensitive detectors in positron imaging. *IEEE* NS-27:569-571, 1980
22. Amsel G, Bosshard R, Zajde C: Shortening of detector signals with passive filters for pile-up reduction. *Nucl Instrum Meth* 71:1-12, 1969
23. Tanaka E, Nohara N, Murayama H: Variable sampling-time technique for improving countrate performance of scintillation detectors. *Nucl Instrum Meth* 158:459-466, 1979
24. Blatt SL, Mahieux J, Kohler D: Elimination of pulse pileup distortion in nuclear radiation spectra. *Nucl Instrum Meth* 60:221-230, 1968
25. Evans RD: *The Atomic Nucleus*, New York, McGraw-Hill, 1955, p 753
26. Mankoff D, Muehllehner G: Multi-frame data acquisition for PET camera using an on-line microprocessor-based system. *IEEE* NS: 1986: in press
27. Tuy HK: Reconstruction of a three-dimensional object from a limited range of views. *J Math Anal Appl* 80:598-616, 1981
28. Tam KC: Multispectral limited-angle reconstruction. *IEEE* NS-30:697-700, 1983
29. Sezan MI, Stark H: Tomographic image reconstruction from incomplete view data by convex projections and direct Fourier inversion. *IEEE* MI-3:91-98, 1094
30. Shepp LA, Vardi Y: Maximum likelihood reconstruction for emission tomography. *IEEE* MI-1:113-122, 1982
31. Shepp LA, Vardi Y, Ra JB, et al: Maximum likelihood PET with real data. *IEEE* NS-31:910-913, 1984
32. Herman GT, Censor Y, Gordon D, et al: Comments on a statistical model for positron emission tomography. *JASA Appl* 80:22-25, 1985
33. Lange K, Carson R: EM reconstruction algorithms for emission and transmission tomography. *JCAT* 8:306-316, 1984
34. Muehllehner G, Karp JS, Guvenis A: A method for reconstructing images from data obtained with a hexagonal bar positron camera. *IEEE Trans Med Imag*: in press
35. Muehllehner G: Effect of resolution improvement on required count density in ECT imaging: A computer simulation. *Phys Med Biol* 30:163-173, 1985
36. Data Spectrum Corporation, Chapel Hill, North Carolina